

# Rotational Components of Normal Modes Measured at a Natural Sandstone Tower (Kane Springs Canyon, Utah, U.S.A.)

Alex Dzubay\*1<sup>®</sup>, Jeffrey R. Moore<sup>1</sup>, Riley Finnegan<sup>1</sup>, Erin K. Jensen<sup>1</sup>, Paul R. Geimer<sup>2</sup>, and Keith D. Koper<sup>1</sup>

### Abstract

Modal analysis of freestanding rock formations is crucial for evaluating their vibrational response to external stimuli, aiding accurate assessment of associated geohazards. Whereas conventional seismometers can be used to measure the translational components of normal modes, recent advances in rotational seismometer technology now allow direct measurement of the rotational components. We deployed a portable, three-component rotational seismometer for a short-duration experiment on a 36 m high sandstone tower located near Moab, Utah, in addition to conducting modal analysis using conventional seismic data and numerical modeling. Spectral analysis of rotation rate data resolved the first three natural frequencies of the tower (2.1, 3.1, and 5.9 Hz), and polarization analysis revealed the orientations of the rotation axes. Modal rotations were the strongest for the first two eigenmodes, which are mutually perpendicular, full-height bending modes with horizontal axes of rotation. The third mode is torsional with rotation about a subvertical axis. Measured natural frequencies and the orientations of displacements and rotation axes match our numerical models closely for these first three modes. In situ measurements of modal rotations are valuable at remote field sites with limited access, and contribute to an improved understanding of modal deformation, material properties, and landform response to vibration stimuli.

Cite this article as Dzubay, A.,
J. R. Moore, R. Finnegan, E. K. Jensen,
P. R. Geimer, and K. D. Koper (2022).
Rotational Components of Normal Modes
Measured at a Natural Sandstone Tower
(Kane Springs Canyon, Utah, U.S.A.), *The*Seismic Record. 2(4), 260–268,
doi: 10.1785/0320220035.

### Introduction

Predicting the vibration response of freestanding rock landforms to seismic, atmospheric, or anthropogenic sources, in support of hazard and conservation management, requires detailed understanding of the natural modes of vibration, including eigenfrequencies and mode shapes (Dowding *et al.*, 1983; Geimer *et al.*, 2020; Finnegan *et al.*, 2021). Recent advances in experimental and numerical modal analysis of rock formations, including arches, towers, and bedrock slope instabilities, have shown that these geological structures exhibit many similarities to civil infrastructure, including bridges and tall buildings (e.g., Brownjohn, 2003; Clinton *et al.*, 2006; Michel *et al.*, 2010). Rock towers (slender in both horizontal dimensions compared to height), in particular, have been shown to exhibit fundamental modes consisting of full-height bending about the slimmest horizontal dimension, followed by a second, perpendicular full-height bending mode, and a third torsional mode with tower rotation about a subvertical axis (Bottelin *et al.*, 2013; Colombero, Godio, and Jongmans, 2021; Finnegan *et al.*, 2022). However, unlike civil structures, rock towers generally lack suitable locations for seismometer arrays, and thus experimental modal analyses are limited by

<sup>1.</sup> Department of Geology and Geophysics, The University of Utah, Salt Lake City, Utah, U.S.A., https://orcid.org/0000-0001-6656-312X (AD); https://orcid.org/0000-0001-5831-2048 (JRM); https://orcid.org/0000-0003-3234-6439 (RF); https://orcid.org/0000-0002-2797-0694 (EKJ); https://orcid.org/0000-0002-9725-6509 (KDK); Los Alamos National Laboratory, Los Alamos, New Mexico, U.S.A., https://orcid.org/0000-0003-2627-5507 (PRG)

<sup>\*</sup>Corresponding author: adzubay@gmail.com

<sup>© 2022.</sup> The Authors. This is an open access article distributed under the terms of the CC-BY license, which permits unrestricted use, distribution, and reproduction in any medium, provided the original work is properly cited.

sparse spatial data. Measurements of mode shapes and spatial gradients of modal deformation are rare.

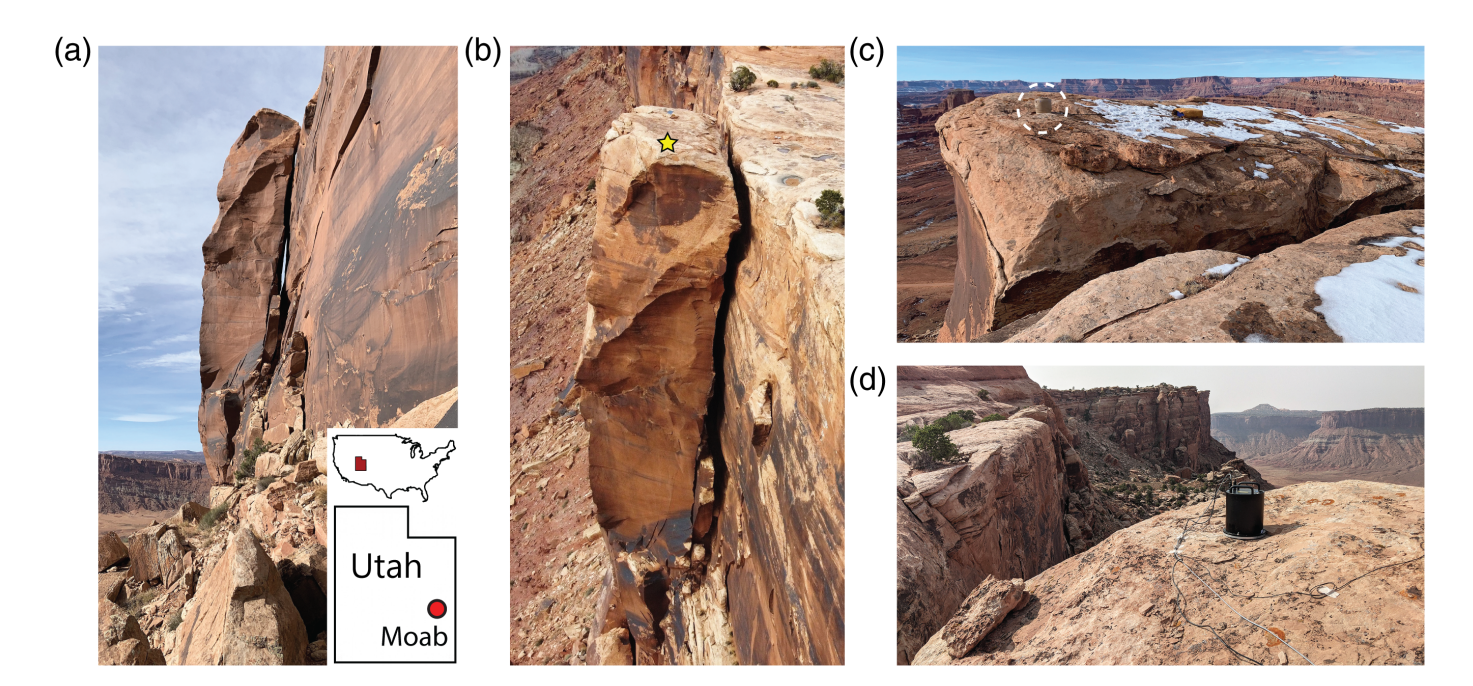
Previous modal analyses of rock landforms have relied on data recorded by conventional (i.e., translational) seismometers (e.g., Lévy et al., 2010; Bottelin et al., 2013; Moore et al., 2016). These data provide details of the eigenmodes at a single point; only in rare cases have seismic array data been used to resolve mode shapes (e.g., Geimer et al., 2020; Häusler et al., 2021; Bessette-Kirton et al., 2022). Translational data alone, however, cannot directly measure rotational motion, and thus most data sets are lacking this component of the deformation field, which can be important for improved characterization of material properties through inversion techniques (Remillieux et al., 2015; Keil et al., 2022; Noe et al., 2022) and for assessing the potential for earthquake-induced damage (e.g., Chandler, 1986; Lee et al., 2009; Igel et al., 2012; Anagnostopoulos et al., 2015). Modal rotations have previously been measured by calculating spatial gradients of motion from seismometer arrays (e.g., Celebi, 2006; Castellani, 2017; Guéguen et al., 2020)—a technique that may suffer from limitations imposed by small measurement areas at most rock landforms. However, recent advances in rotational seismometer technology based on fiber-optical gyroscopes (Bernauer et al., 2018) now allow direct in situ measurement of modal rotations (Guéguen et al., 2020), data that can provide missing details of modal deformation fields aiding improved structural characterization and damage monitoring. Such data can be especially valuable when experimental conditions preclude deployment of large sensor arrays.

In this study, we present new ambient vibration data from both translational and rotational seismometers placed atop a slender rock tower located near Moab, Utah. These data sets are interrogated for modal analysis and compared: translation data provide eigenfrequency and eigenvector information, whereas rotation data reveal rotational components of the eigenmodes and orientations of the modal rotation axes. Our results are the first to use direct measurement of modal rotations at a natural rock landform and are verified by numerical modeling. The incorporation of rotation measurements in modal analysis has the capacity to improve measurement of complex mode shapes, describe elastic material properties, and validate theoretical models, contributing to improved understanding of landform response to vibrational forcing. Such information is important in evaluating the stability and the potential for damage of culturally valued rock landforms (e.g., Moore et al., 2016), including rock towers and arches, as well as monitoring structural change through passive ambient vibration techniques.

# Study Site and Experiments

Our study site (Fig. 1a) is a 36 m high rock tower located 17 km southwest of Moab, Utah, in Kane Springs Canyon (latitude: 38.48172°, longitude: -109.59498°). The tower (termed Kane Springs Ledge Tower) is composed of massive, monolithic Jurassic Wingate sandstone and formed through partial collapse of rock slabs from an extended cliff trending at an azimuth of 338° (328° from magnetic north). It is ~5 m thick and ~13 m across, with approximately prismatic geometry. Accessing the top of the tower requires scrambling 300 vertical meters up steep boulders and colluvium of an ancient landslide, then crossing an ~1 m wide open crack separating the tower from the cliff. This open crack extends downward 20 m, where it becomes filled with fallen rock and eventually fully closes toward the base of the tower. The top surface of the tower is relatively flat, tilting slightly to the southeast, which together with natural undulations of the rock surface limit suitably flat areas to deploy seismometers (Fig. 1b).

We analyze data from two short-term experiments that were spatially collocated (station code KSLTA, see star in Fig. 1b) but separated in time by 8 months: (1) We deployed a Nanometrics Trillium Compact 20 s (TC-20) three-component seismometer with 24-bit Centaur data logger on 16 January 2021, continuously measuring ambient vibration velocity data at 100 Hz for approximately 23 hr (Fig. 1c). (2) We deployed an iXblue blueSeis-3A (BS-3A) three-component rotational seismometer, paired with a DiGOS C-CUBE, recording ambient rotation rate at 200 Hz for five hours on 10 August 2021 (Fig. 1d; see Data and Resources). Unfortunately, due to unknown reasons possibly related to high temperatures during the measurement or a poor cable connection, only 40 min of useable data were obtained in the latter deployment. In addition to these experiments, we separately installed a Trillium Compact seismometer and Centaur datalogger continuously recording 50 Hz ambient vibration data at a point in the center of the tower on 20 February 2021, with data collection still ongoing. The location was selected for instrument safety and is sufficiently different from our two short-term deployments to preclude polarization comparison. We use data from this monitoring station only to link natural frequencies measured with different instruments at different times, as these drift slightly throughout the year with changing temperatures (e.g., Bottelin et al., 2013; Geimer et al., 2022). All seismometers were set on the bare rock surface, leveled, and aligned to magnetic north using a hand compass (estimated accuracy ± 5°). TC-20 seismometers were



covered with a bucket to mitigate wind buffeting, while the larger BS-3A was left uncovered (Fig. 1). Because of demanding site access, it was not possible to collocate TC-20 and BS-3A instruments during the same measurement period.

### Methods

We processed all ambient seismic data (i.e., both translational and rotational) in a similar manner to determine spectral and polarization attributes. Trillium Compact data were demeaned, detrended, instrument-corrected, and band-pass filtered between 0.1 and 15 Hz to analyze relevant velocity data in m/s. Raw blueSeis data were first "deramped" by the manufacturer—a procedure that removes signals from operation of the fiber-optical gyroscope. The instrument has a flat transfer function from DC to 50 Hz, with a scaling factor that is relatively insensitive to temperature changes (Bernauer et al., 2018). Scaled data were demeaned to remove the DC component of the signal related to rotation of the Earth, detrended, and then band-pass filtered between 0.1 and 15 Hz to analyze rotation rate in nrad/s. For TC-20 data, we selected a representative hour with low wind and few anthropogenic disturbances between 01:00 and 02:00 UTC on 17 January 2021 (6 p.m. local time on 16 January 2021). For BS-3A data, we used all available data between 15:16 and 15:52 UTC (9 a.m. local time) on 10 August 2021. This time block included a short gap while we checked the data stream, which we removed from further processing.

We computed the power spectral density (PSD) for each data set separately using fast Fourier transforms (FFT) over

**Figure 1.** Overview of study site and seismometer deployments. (a) Lateral view of the sandstone tower located in Kane Springs Canyon, near Moab, Utah, U.S.A. (inset map). The tower is approximately 36 m high, 13 m wide, and 5 m thick. Although not visible, the rear crack is fully penetrating through the upper ~20 m of the tower. (b) Aerial view of the tower showing open rear crack and location of the seismometer deployments (yellow star). (c) TC-20 translational seismometer deployed in January 2021 (dashed circle added for clarity). (d) BS-3A rotational seismometer deployed in the same position in August 2021.

selected time blocks to generate  $3 \times 3$  spectral matrices (Koper and Burlacu, 2015). Because of varying sampling rates, the number of points per FFT window were 2048 (TC-20) and 4096 (BS-3A). We then averaged the spectra from 80% overlapped, Hanning-tapered windows. For polarization analysis, we computed polarization attributes at selected frequencies (Koper and Hawley, 2010; Incorporated Research Institutions for Seismology Data Management Center [IRIS DMC], 2015) using the same window parameters as the PSDs. We determined the degree of polarization ( $\beta^2$ ; dimensionless ranging from 0 to 1; Samson, 1983), the polarization orientation in the horizontal plane (degrees from magnetic north), as well as the incidence angle (degrees from vertical). We applied this workflow to both TC-20 and BS-3A data. For the translational data, highly polarized ground motion corresponding to spectral peaks visible in PSD curves reveals the natural modes of the tower, and the polarization orientations describe particle motion at the sensor location. For rotational data, polarization

and PSD peaks again correspond to natural modes of the tower, but the azimuth and incidence values now describe the orientation of the rotation axis for each mode.

We created a 3D model of the tower using the program Blender based on field measurements (tape measure and TruPulse 360 laser rangefinder) as well as ground observations and photographs. Various field visits provided opportunity to access the base and all sides of the tower to allow detailed inspection and measurement. The scaled 3D geometry was first coarsely sketched in Blender and then carefully sculpted to account for local geometric details on all visible faces. The rear fracture was extended in a planar manner downward to the base of the tower, reflecting the obscured intact rock contact with the adjoining cliff. The base of the tower was placed at a stratigraphic interface in the Wingate Sandstone just above the contact with the underlying (and slope forming) Chinle Formation.

Following methods of Moore et al. (2019) and Finnegan et al. (2022), we performed finite-element numerical modal analysis using COMSOL Multiphysics (see Data and Resources). The analysis outputs the eigenfrequencies of the tower and associated 3D modal deformation fields. As both this tower and Castleton Tower studied previously by Moore et al. (2019) are composed of Wingate sandstone, we implemented the same uniform density ( $\rho$ ) of 2200 kg/m<sup>3</sup>. Next, providing simple boundary conditions with the tower fixed at its base and up to 16 m on its northeastern side (as determined from field inspection), we adjusted the value for Young's modulus (E) until the predicted eigenfrequencies matched the natural frequencies observed in the data. We extracted modeled deflections at the sensor location, computing modal displacement vectors to compare with polarization of the translational data and the curl of modal displacement to compare with orientations from the rotational data. Natural frequencies can drift throughout the year, as temperature variations affect the stiffness of the rock mass (e.g., Bottelin et al., 2013; Colombero, Godio, and Jongmans, 2021; Colombero et al., 2021; Geimer et al., 2022). Therefore, we allowed E to vary slightly in our analysis matching frequencies measured during summer versus winter.

## **Results**

Spectral analysis of translational seismic data revealed clear indications of up to six normal modes of the tower (Fig. 2a). At the time of measurement in January 2021, these occurred at frequencies of 1.8, 2.8, 5.1, 7.4, 9.1, and 10.5 Hz. Polarization values ( $\beta^2$ ) were nearly 1 for the first three modes, dropping to a low of 0.6 at mode 5. Ground motion was oriented roughly

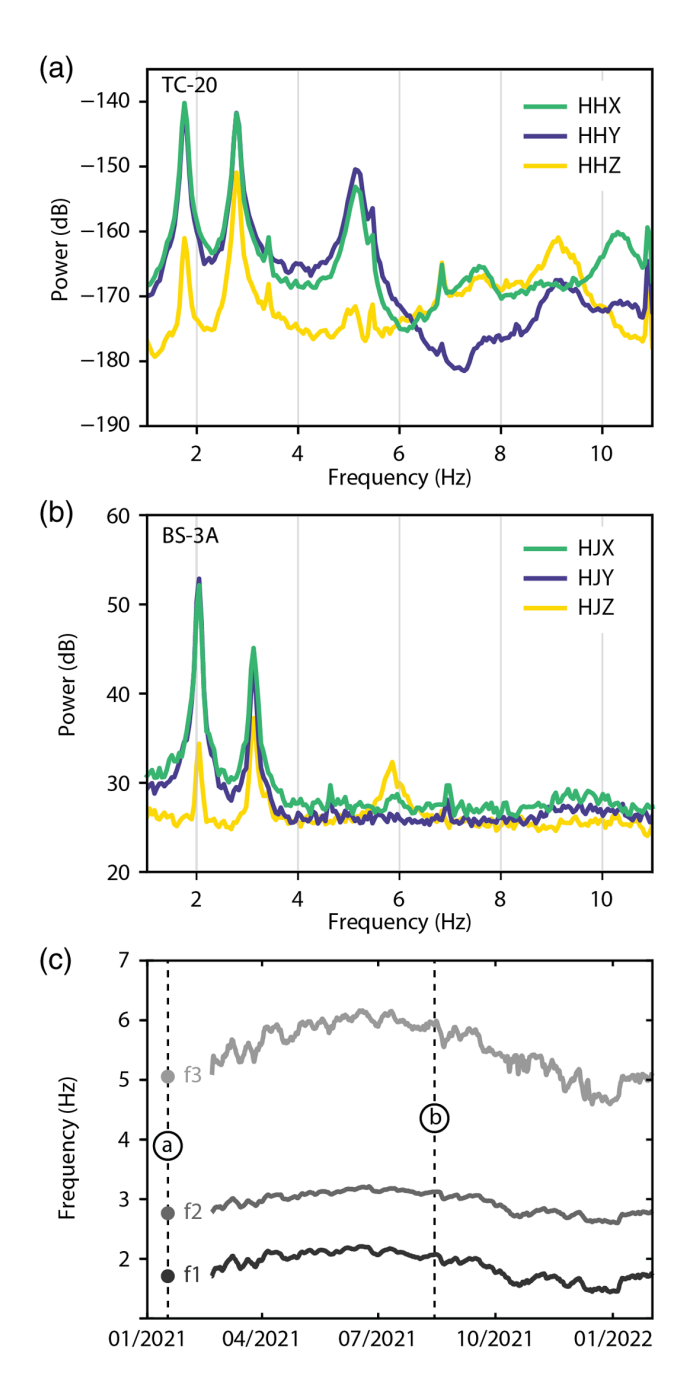


**Figure 2.** Spectral data from seismometer deployments. (a) TC-20 ambient vibration spectra from 01:00 to 02:00 UTC on 17 January 2021. Components are east, north, and vertical (HHX, HHY, HHZ, respectively) relative to magnetic north. Velocity power spectral density is shown in decibel power relative to 1 m<sup>2</sup>s<sup>-2</sup> Hz<sup>-1</sup>. (b) BS-3A rotational seismic data from 15:16 to 15:52 UTC on 10 August 2021. Rotation power spectral density is shown in decibel power relative to 1 nrad<sup>2</sup>s<sup>-2</sup> Hz<sup>-1</sup>. Components are rotation about east and north horizontal axes (HJX, HJY, respectively), and the vertical axis (HJZ). (c) Frequency drift over time for the first three modes (f1, f2, and f3) from a seismometer installed at the center of the tower. Frequencies drift over the year with changing temperatures. The dashed vertical lines mark the times of measurements shown in (a) and (b).

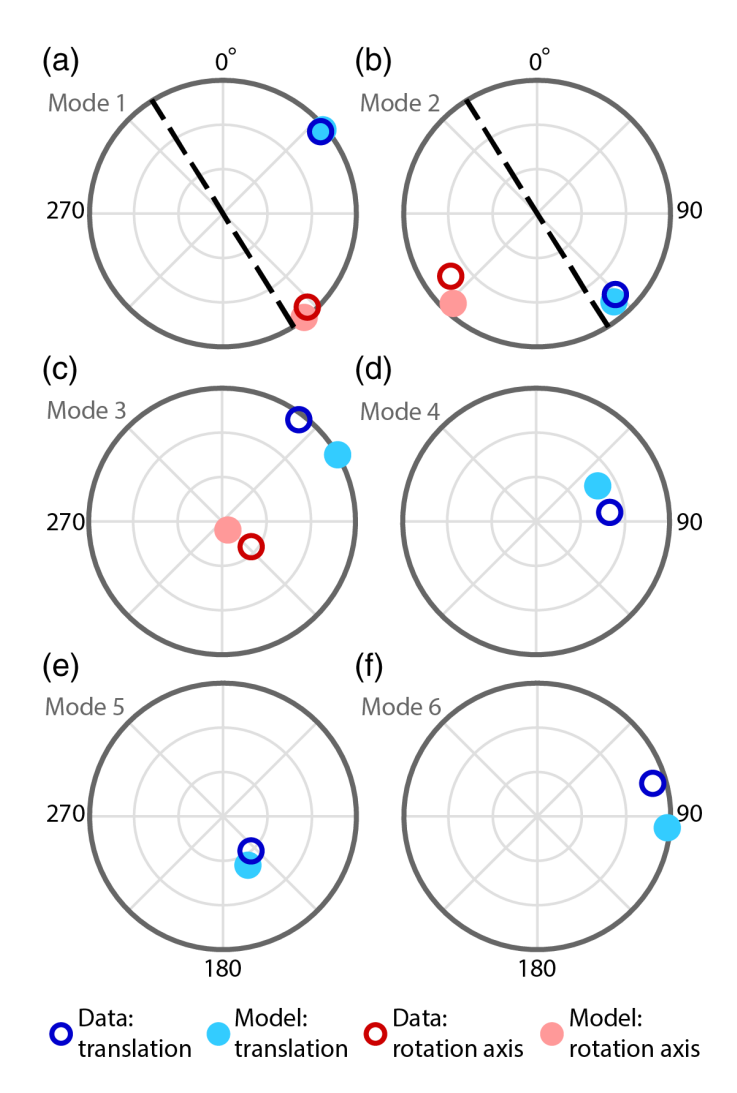


**Figure 3.** Polarization results from measurements and modeling. (a)–(f) Polar plots comparing measured and modeled polarization vectors and rotation axes for the first six modes of vibration (rotation data only available for modes 1–3). Radial coordinates are incidence angle (vertical at center and horizontal at the perimeter), and angular coordinates show azimuth with 0° = magnetic north. The tower is oriented with its longer horizontal dimension trending 328° (parallel to the cliff): see bold dashed lines in panels (a) and (b).

parallel to the narrowest horizontal axis of the tower for the first mode and aligned with the wider horizontal axis for the second mode, as expected for full-height bending. Other modes showed slightly more irregular orientations (Fig. 3).

Spectral peaks associated with the first three natural modes of the tower were also clearly visible in BS-3A rotation rate data (Fig 2b). At the time of measurement in August 2021, these frequencies had drifted to slightly higher values of 2.1, 3.1, and 5.9 Hz, an increase of 17%, 11%, and 16%, respectively

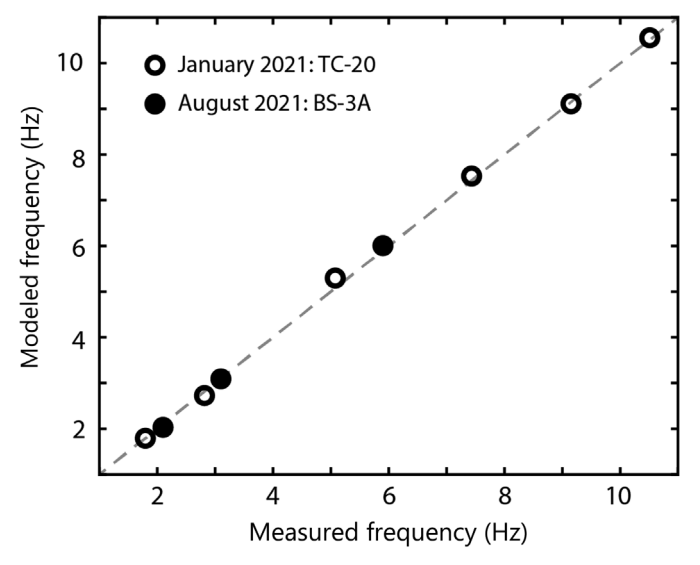
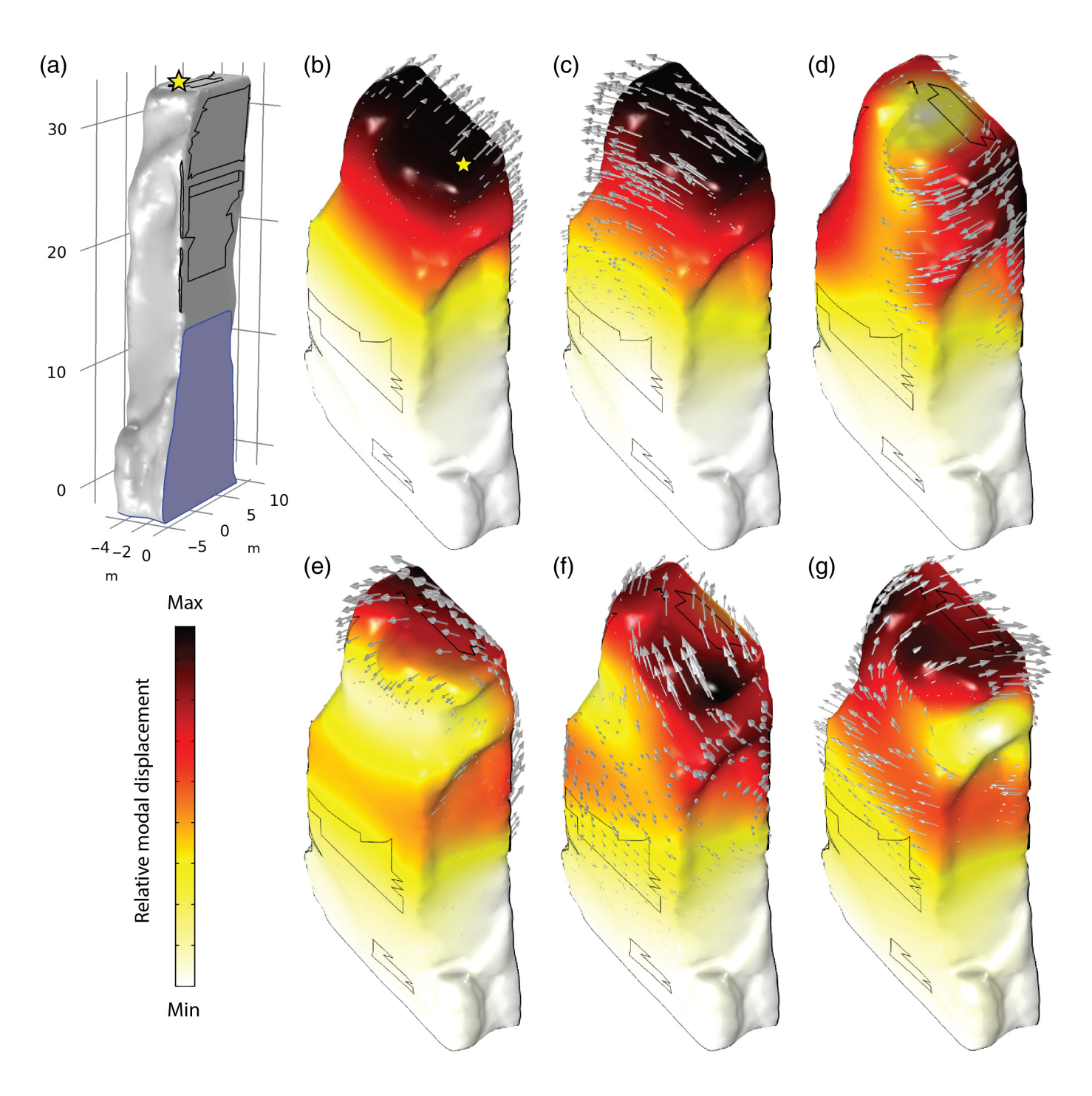


**Figure 4.** Comparison of measured and modeled frequencies from the two seismometer deployments. The dashed line is 1:1 trend indicating a perfect match. Measured frequencies drift upward by an average of 14% with changing temperatures during the year, which is modeled by increasing Young's modulus from 1.4 to 1.8 GPa.

(compare to Colombero *et al.*, 2021; Geimer *et al.*, 2022). Figure 2c shows the monitored variation of the first three modal frequencies over time, with our two measurements also indicated, demonstrating that the measured drifts are within the expected seasonal range for this tower. Spectral peaks associated with higher modes (4–6) were not visible in the rotational data. Polarization values for the first two modes approached 1, whereas the third mode dropped steeply to 0.3. Polarization orientations revealed that the first two modes have subhorizontal axes of rotation with mutually perpendicular orientations: the first rotation axis trends perpendicular to the narrowest tower width, whereas the second is perpendicular to the wider horizontal axis. The third mode has a vertically oriented rotation axis, as expected for a torsional mode.

Results of numerical modal analysis are shown in Figures 4 and 5. Implementing a Young's modulus of 1.4 GPa closely reproduced the six modal frequencies identified in TC-20 data, with a mean absolute difference of less than 2% (Fig. 4). Accounting for seasonal frequency drift, *E* increased to 1.8 GPa to match the summer rotational data (mean frequency variation <1%). Both Young's modulus values are well within the expected range for sandstones in the region (Geimer *et al.*, 2020). Modeled eigenvector orientations matched measurements from the translational data closely, with an average mismatch of 14°



for azimuth and 4° for incidence across all six modes (Fig. 3). Similarly, modeled curls closely matched rotation axis orientations, with an average mismatch of 10° for azimuth and 11° for incidence across the three resolved modes. The close match between modeled and measured frequencies and orientations indicates that our model is appropriately parameterized, supporting our assumptions of uniform material properties and boundary conditions (Fig. 5a). The full modal deformation fields

**Figure 5.** Numerical modal analysis of the Kane Springs Ledge tower. (a) Geometry and boundary conditions. The blue shaded polygon is the fixed rear boundary where the tower adheres to the cliff; yellow star is the field measurement location. (b)–(g) First six modes of vibration, with color map and arrows illustrating deformation at zero phase (normalized relative scale for each mode).

are shown in Figure 5, confirming that the first two modes are full-height bending in mutually perpendicular directions aligned with the thinnest and thicker horizontal widths of the tower. The third mode is torsional with a subvertical rotation axis, whereas modes 4–6 are more complex second-order and possibly third-order bending modes.

### Discussion

Our experimental data demonstrated that a three-component fiber-optical gyroscope rotational seismometer can measure the rotational components of modal deflection of a 36 m high sandstone tower. Although direct measurements of modal rotations in buildings are themselves rare (e.g., Guéguen et al., 2020; Lin et al., 2012), to our knowledge this is the first time modal rotations that have been directly measured on a rock landform. Rotation rate data from the BS-3A instrument were output in standard miniSEED format and processed using identical routines as used for the translational seismic data, that is, no additional or new processing codes were needed to analyze the rotational data. We note that fiber-optical gyroscope instruments have also recently been successfully used to measure ground rotations in other seismology investigations, for example, with applications in volcanology (Eibl et al., 2022; Wassermann et al., 2022).

Although we were able to detect and characterize six modes of vibration of the tower from TC-20 data, rotational measurements from the BS-3A only revealed three modes (compare Figs. 2a,b), likely due to the excitation levels of modes 4-6 not being above detectable limits of the sensor. The BS-3A instrument is among the most sensitive portable rotation sensors available, with self-noise in the range of  $\sim 10-20 \text{ nrad/s/}\sqrt{\text{Hz}}$ (Bernauer et al., 2018), however, our data show that spectral information at mode 3 is just above the instrument noise floor, suggesting that any rotational motions associated with modes 4-6 are undetectable in our dataset. Ways to lower the noise floor in the field might include covering the sensor to avoid wind contact (as is standard for our TC-20 deployments). Data from higher excitation time periods, for example, shaking from earthquakes, might also have been recorded during a longer deployment, making the higher modes detectable in rotational data.

Prior to the experiment, we hypothesized that modal rotations would be greatest for the torsional mode of the tower—mode 3; however, our data revealed that rotation rate had the greatest amplitude at the first two full-height bending modes. Moore *et al.* (2019) and Finnegan *et al.* (2022) established that slender rock towers, such as this, exhibit Euler–Bernoulli bending modes akin

to a cantilever, in contrast to shear deformation more common in buildings. Rotations are expected for Euler–Bernoulli bending, whereas they might be less pronounced for shear deformation, suggesting that measurement of rotations could be an experimental means to assess theoretical models of modal deflection. Modal mass participation factors resolved from our numerical analysis additionally show that modes 1 and 2 incorporate  $\sim 30\%$  effective modal mass in their respective orientations, whereas mode 3 has less than 2% effective modal mass, suggesting that the first two modes likely dominate the resolved ambient vibration spectra.

Comparison of eigenvector orientations with modal rotation axes revealed expected trends. For modes 1 and 2, we found that the modal rotation axes are oriented perpendicular to the modal displacement directions, each having horizontal incidence angles, as expected for first-order bending modes (Figs. 3 and 5). Meanwhile, the torsional mode has a subvertical rotation axis nearly perpendicular to the incidence angle of the modal displacement vector (Fig. 3c). This ~90° difference might be a revealing metric for torsional motion from instrumental data alone, as identifying torsional modes from sparse translational seismometer deployments is often not possible without numerical modeling (e.g., Finnegan *et al.*, 2022). The addition of a rotational seismometer, in combination with translational seismic data, may thus uniquely allow for identification of torsional modes from field data.

Rotational seismic data have been shown to contribute unique information relevant for damage detection in structural health monitoring applications (Doebling et al., 1998; Bońkowski et al., 2020; Huseynov et al., 2020). To explore the sensitivity of rotational polarization metrics to damage, as compared to translational values, we conducted a series of simulations using our model of the Kane Springs Ledge Tower. We created three horizontal domains layered through the middle of the tower—each 5 m high and located in areas experiencing large strains for the first modes. We then simulated damage by softening each layer in turn, reducing the Young's modulus by half to 0.7 GPa, and calculated the resulting polarization parameters for both translation and rotation. Results showed that the torsional mode (mode 3), in particular, exhibited notable changes in azimuth of the rotation axis when softening the different layers (10°, 7°, and 11° for the bottom, middle, and top layers, respectively), whereas translational vector orientations were less affected (azimuth change of 1° to 3° over all models). These preliminary tests suggest that polarization parameters calculated from rotational seismic data

may be more sensitive to material changes caused by damage than corresponding translational polarization metrics.

The addition of rotational seismic data may also add new information useful for material characterization, such as describing the material stiffness tensor from inversion of experimental modal analysis data or improving characterization of complex structures consisting of multiple materials (Doebling et al., 1998; Remillieux et al., 2015; Noe et al., 2022). Moreover, rotational data can add new information useful for seismic stability analyses, for example, showing how rock landforms rotate during earthquakes and allowing calculation of rotational strains, or revealing the degree of excitation of torsional modes from different energy inputs (Anagnostopoulos et al., 2015). With recent advances in seismometer technology, rotational seismic data and resulting descriptions of the rotational components and response of normal modes stand to become increasingly common in applications relating to characterization and structural health monitoring of unstable rock formations and landslides, benefiting geohazard analysis, infrastructure and resource protection, and public safety.

### Conclusions

We deployed a portable blueSeis-3A rotational seismometer to measure rotations associated with the normal modes of a 36 m high sandstone tower located near Moab, Utah. The results compared well with seismic data from the same location generated using a translational seismometer (Trillium Compact 20-s). Although TC-20 data revealed six modes of vibration of the tower, BS-3A data could only conclusively characterize three in our deployment, likely related to low excitation levels of higher order modes. Processing both data sets for polarization information revealed consistent trends: for modes 1 and 2, rotation axes are horizontal and perpendicular to the displacement azimuth, as expected for first-order bending modes, whereas the third mode has a subvertical rotation axis perpendicular to the incidence angle of modal displacement. These results indicate that the first two modes represent Euler-Bernoulli bending and the third mode is torsion. Direct measurements of rotation are needed to identify torsional modes in most cases at natural rock landforms where deployment of dense sensor arrays is rarely feasible. Incorporation of rotational data in future experiments stands to benefit material and structural characterization, assessment of seismic stability, as well as damage assessment and monitoring supporting landform conservation and hazard management.

### **Data and Resources**

Data generated in this study are available for download at doi: 10.7914/SN/5P\_2013.

# **Declaration of Competing Interests**

The authors acknowledge that there are no conflicts of interest recorded.

# Acknowledgments

The authors gratefully acknowledge iXblue for use of the blueSeis-3A rotational seismometer as well as subsequent support from Frédéric Guattari with the deramping procedure. Oliver Moore provided invaluable field assistance. The authors thank two anonymous reviewers for helpful comments that improved this article. This study was funded by the National Science Foundation Award Number 2150896 and by the University of Utah Office of Undergraduate Research.

### References

- Anagnostopoulos, S. A., M. T. Kyrkos, and K. G. Stathopoulos (2015). Earthquake induced torsion in buildings: Critical review and state of the art, *Earthq. Struct.* **8**, no. 2, 305–377.
- Bernauer, F., J. Wassermann, F. Guattari, A. Frenois, A. Bigueur, A. Gaillot, E. Toldide, D. Ponceau, U. Schreiber, and H. Igel (2018). BlueSeis3A: Full characterization of a 3C broadband rotational seismometer, *Seismol. Res. Lett.* **89**, no. 2A, 620–629.
- Bessette-Kirton, E. K., J. R. Moore, P. R. Geimer, R. Finnegan, M. Häusler, and A. Dzubay (2022). Structural characterization of a toppling rock slab from array-based ambient vibration measurements and numerical modal analysis, *J. Geophys. Res. Earth Surf.* **127**, no. 8, e2022JF006679.
- Bońkowski, P. A., P. Bobra, Z. Zembaty, and B. Jędraszak (2020). Application of rotation rate sensors in modal and vibration analyses of reinforced concrete beams, *Sensors* **20**, no. 17, 4711.
- Bottelin, P., C. Levy, L. Baillet, D. Jongmans, and P. Guéguen (2013). Modal and thermal analysis of Les Arches unstable rock column (Vercors massif, French Alps), *Geophys. J. Int.* **194**, no. 2, 849–858.
- Brownjohn, J. M. (2003). Ambient vibration studies for system identification of tall buildings, *Earthq. Eng. Struct. Dynam.* **32**, no. 1, 71–95.
- Castellani, A. (2017). Array-derived rotational seismic motions: Revisited, *Bull. Earthq. Eng.* **15**, no. 3, 813–825.
- Çelebi, M. (2006). Recorded earthquake responses from the integrated seismic monitoring network of the Atwood building, Anchorage, Alaska, *Earthq. Spectra* **22**, no. 4, 847–864.
- Chandler, A. M. (1986). Building damage in Mexico City earthquake, *Nature* **320**, no. 6062, 497–501.
- Clinton, J., S. C. Bradford, T. H. Heaton, and J. Favela (2006). The observed wander of natural frequencies in a structure, *Bull. Seismol. Soc. Am.* 96, no. 1, 237–257.

- Colombero, C., A. Godio, and D. Jongmans (2021). Ambient seismic noise and microseismicity monitoring of a prone-to-fall Quartzite Tower (Ormea, NW Italy), *Remote Sens.* **13**, no. 9, 1664.
- Colombero, C., D. Jongmans, S. Fiolleau, J. Valentin, L. Baillet, and G. Bièvre (2021). Seismic noise parameters as indicators of reversible modifications in slope stability: A review, *Surv. Geophys.* 42, no. 2, 339–375.
- Doebling, S. W., C. R. Farrar, and M. B. Prime (1998). A summary review of vibration-based damage identification methods, *Shock Vib. Digest* **30**, no. 2, 91–105.
- Dowding, C. H., F. S. Kendorski, and R. A. Cummings (1983). Response of rock pinnacles to blasting vibrations and airblasts, *Bull. Assoc. Eng. Geol.* **20**, no. 3, 271–281.
- Eibl, E. P., M. Rosskopf, M. Sciotto, G. Currenti, G. GraziaDi, P. Jousset, F. Krüger, and M. Weber (2022). Performance of a rotational sensor to Decipher volcano seismic signals on Etna, Italy, *J. Geophys. Res.* **127**, no. 6, e2021JB023617.
- Finnegan, R., J. R. Moore, and P. R. Geimer (2021). Vibration of natural rock arches and towers excited by helicopter-sourced infrasound, *Earth Surf. Dynam.* **9**, no. 6, 1459–1479.
- Finnegan, R., J. R. Moore, P. R. Geimer, A. Dzubay, E. K. Bessette-Kirton, J. Bodtker, and K. Vollinger (2022). Ambient vibration modal analysis of Natural Rock Towers and Fins, Seismol. Res. Lett. 93, no. 3, 1777–1786.
- Geimer, P. R., R. Finnegan, and J. R. Moore (2020). Sparse ambient resonance measurements reveal dynamic properties of freestanding rock arches, *Geophys. Res. Lett.* **47**, no. 9, e2020GL087239.
- Geimer, P. R., R. Finnegan, and J. R. Moore (2022). Meteorological controls on reversible resonance changes in Natural Rock Arches, *J. Geophys. Res. Earth Surf.* **127**, no. 10, e2022JF006734.
- Guéguen, P., F. Guattari, C. Aubert, and T. Laudat (2020). Comparing direct observation of torsion with array-derived rotation in civil engineering structures, Sensors 21, no. 1, 142.
- Häusler, M., P. R. Geimer, R. Finnegan, D. Fäh, and J. R. Moore (2021). An update on techniques to assess normal-mode behavior of rock arches by ambient vibrations, *Earth Surf. Dynam.* **9**, no. 6, 1441–1457.
- Huseynov, F., C. Kim, E. J. Obrien, J. M. W. Brownjohn, D. Hester, and K. C. Chang (2020). Bridge damage detection using rotation measurements—Experimental validation, *Mech. Syst. Signal Process.* 135, 106,380.
- Igel, H., J. Brokesova, J. Evans, and Z. Zembaty (2012). Preface to the special issue on "Advances in rotational seismology: Instrumentation, theory, observations, and engineering," J. Seismol. 16, 571–572.
- Incorporated Research Institutions for Seismology Data Management Center (IRIS) (DMC) (2015), Data services products: Polarization attributes bundle, doi: 10.17611/DP/NTK.4.

- Keil, S., A. Wilczek, J. Wassermann, and S. Kremers (2022). Comparing single-station 6C measurements and array measurements for seismic microzonation in Munich, Germany, *Geophys. J. Int.* 231, no. 3, 1634–1652.
- Koper, K. D., and R. Burlacu (2015). The fine structure of double-frequency microseisms recorded by seismometers in North America, J. Geophys. Res. Solid Earth 120, no. 3, 1677–1691.
- Koper, K. D., and V. L. Hawley (2010). Frequency dependent polarization analysis of ambient seismic noise recorded at a broadband seismometer in the central United States, *Earthq. Sci.* **23**, no. 5, 439–447.
- Lee, W. H. K., H. Igel, and M. D. Trifunac, (2009). Recent advances in rotational seismology, *Seismol. Res. Lett.* **80**, no. 3, 479–490.
- Lévy, C., L. Baillet, D. Jongmans, P. Mourot, and D. Hantz, (2010). Dynamic response of the Chamousset rock column (Western Alps, France), J. Geophys. Res. Earth Surf. 115, F04043, doi: 10.1029/2009JF001606.
- Lin, C. J., W. G. Huang, H. P. Huang, B. S. Huang, C. S. Ku, and C. C. Liu (2012). Investigation of array-derived rotation in TAIPEI 101, J. Seismol. 16, no. 4, 721–731.
- Michel, C., P. Guéguen, S. AremEl, J. Mazars, and P. Kotronis (2010).
  Full-scale dynamic response of an RC building under weak seismic motions using earthquake recordings, ambient vibrations and modeling, *Earthq. Eng. Struct. Dynam.* 39, no. 4, 419–441.
- Moore, J. R., P. R. Geimer, R. Finnegan, and C. Michel (2019). Dynamic analysis of a large freestanding rock tower (Castleton Tower, Utah), *Bull. Seismol. Soc. Am.* **109**, no. 5, 2125–2131.
- Moore, J. R., M. S. Thorne, K. D. Koper, J. R. Wood, K. Goddard, R. Burlacu, S. Doyle, E. Stanfield, and B. White (2016). Anthropogenic sources stimulate resonance of a natural rock bridge, *Geophys. Res. Lett.* **43**, no. 18, 9669–9676.
- Noe, S., S. Yuan, J. P. Montagner, and H. Igel (2022). Anisotropic elastic parameter estimation from multicomponent ground-motion observations: A theoretical study, *Geophys. J. Int.* **229**, no. 2, 1462–1473.
- Remillieux, M. C., T. J. Ulrich, C. Payan, J. Rivière, C. R. Lake, and P.-Y. Le Bas (2015). Resonant ultrasound spectroscopy for materials with high damping and samples of arbitrary geometry, *J. Geophys. Res.* **120**, no. 7, 4898–4916.
- Samson, J. C. (1983). Pure states, polarized waves, and principal components in the spectra of multiple, geophysical time-series, *Geophys. J. Roy. Astron. Soc.* **72**, 647–664.
- Wassermann, J., T. Braun, M. Ripepe, F. Bernauer, F. Guattari, and H. Igel (2022). The use of 6DOF measurement in volcano seismology—A first application to Stromboli volcano, *J. Volcanol. Geotherm. Res.* **424**, 107,499.

Manuscript received 30 September 2022
Published online 1 December 2022